Journal of Environmental Chemical Engineering 8 (2020) 104069

Contents lists available at ScienceDirect

Journal of Environmental Chemical Engineering

journal homepage: www.elsevier.com/locate/jece

Novel Insights into Activated Carbon Derived from Municipal Solid Waste for CO_2 Uptake: Synthesis, Adsorption Isotherms and Scale-up

Mohsen Karimi[a,b,*], Lucas F.A.S. Zafanelli[b], João P.P. Almeida[c], Gylles R. Ströher[d], Alírio E. Rodrigues[a], José A.C. Silva[b,*]

[a] Laboratory of Separation and Reaction Engineering (LSRE), Associate Laboratory LSRE/LCM, Department of Chemical Engineering, Faculty of Engineering, University of Porto, Rua Dr. Roberto Frias, S/N, 4099-002, Porto, Portugal
[b] Centro de Investigação de Montanha (CIMO), Instituto Politécnico de Bragança, Campus de Santa Apolónia, 5300-253 Bragança, Portugal
[c] Centro de Investigação em Digitalização e Robótica Inteligente(CEDRI), Instituto Politécnico de Bragança, Campus de Santa Apolónia, 5300-253 Bragança, Portugal
[d] Department of Chemical Engineering, Federal University of Technology—Paraná, Rua Marcílio Dias, 635, CEP 86.812-460, Apucarana, Paraná, Brazil

ARTICLE INFO

Editor:Teik Thye Lim

Keywords:
Global Warming
Wastes Management
Fixed Bed Adsorption
Mathematical Modeling
Pressure Swing Adsorption

ABSTRACT

Recently, developing bio-based carbon materials due to the surface chemistry and a large spectrum of pore structures have received much attention. In the present work, a series of activated carbon (AC) adsorbents were synthesized from the compost derived by the mechanical/biological treatment of municipal solid wastes and evaluated regarding their CO_2 uptake. The AC samples were characterized by sulfuric acid and calcination by N_2 at 400 and 800 °C. Then, the CO_2 uptake capacities were evaluated by dynamic breakthrough experiments in a temperature range of 40-100 °C and pressures up to 3 bar. The presented data were properly described by Langmuir model and it was revealed that the CMSW-S-800 sample, treated with sulfuric acid and activated at 800 °C, has the highest CO_2 uptake capacity with an amount adsorbed around 2.6 mol/kg at 40 °C. In the next step, a mathematical model has been developed to match the experimental dynamic breakthrough data and design a pressure swing adsorption (PSA) cyclic process to evaluate the capacity and potential of the best AC sample for CO_2 adsorption. The results arising from this work showed a possible route for the application of the compost as a source of activated carbon for the sorption of greenhouse gases.

1. Introduction

Climate change is today a major environmental concern, especially due to the large emissions of greenhouse gases. According to reports, by rising level of greenhouse gases (GHGs) [1], the surface temperature of the planet will increase between 3-5 °C by the end of the century, which will have catastrophic effects on the ecosystem. This ecological problem has been originated from anthropogenic activities which undoubtedly, fossil fuel industries and coal fired power plants have a main rule on GHGs emission [2,3]. In this way, carbon capture and sequestration (CCS) strategy, as a combination of several technologies, has emerged which is a promising policy for reduction of CO_2 emission [4]. To this end, CO_2 trapping occurs in three different steps including pre-combustion, post-combustion and oxy-fuel combustion [5]. Among these processes, post-combustion technique is widely considered for CO_2 capture in the flue gases of different industries [6]. It is worth mentioning, the flue gases consists around 10-15 vol% CO_2 in the temperature range of 40 −60 °C, which is the main element of global warming [5,7].

Currently, various classes of adsorbents including carbons based materials [4,7,8], zeolite molecular sieves [9,10], metal organic frameworks [11,12], meso-porous silicons [13,14] and other ones [15,16] have been extensively investigated for separation processes, energy conversion, and catalysis. Among different developed materials, activated carbons (ACs) are highly favorable adsorbents for CO_2 adsorption for several reasons [17]. First, these materials have a high uptake capacity accompanied with rapid adsorption kinetics [18]. Also, ACs have a hydrophobic property that is one of the main benefit of these materials relatively to other ones, which contributes to the resistance quality of ACs over the presence of moisture [19]. In addition, abundant resources of ACs (including: carbon-containing fly ash, resins or biomass) nominate them as a cheap adsorbent [20]. Recently several studies have devoted to evaluate the potential of different waste materials [21,22]. In this way, Bhatta et al. [23] developed low cost activated carbons

* Corresponding author at: Laboratory of Separation and Reaction Engineering (LSRE), Associate Laboratory LSRE/LCM, Department of Chemical Engineering, Faculty of Engineering, University of Porto, Rua Dr. Roberto Frias, S/N, 4099-002, Porto, Portugal.
E-mail addresses: mohsen.karimi@fe.up.pt (M. Karimi), jsilva@ipb.pt (J.A.C. Silva).

https://doi.org/10.1016/j.jece.2020.104069
Received 3 March 2020; Received in revised form 23 April 2020; Accepted 16 May 2020
Available online 21 May 2020

Nomenclature

a_p	specific area of the pellet (m^{-1})
a_c	specific area of the column (m^{-1})
C	total gas concentration (mol m^{-3})
C_{pg}	heat capacity of gas (J mol^{-1} K^{-1})
C_{ps}	heat capacity of solid (J mol^{-1} K^{-1})
d_p	Pellet diameter (m)
d_c	column diameter (m)
D_{ax}	axial mass dispersion coefficient (m^2 s^{-1})
D_m	effective molecular diffusivity (m^2 s^{-1})
D_p	pore diffusivity (m^2 s^{-1})
D_k	Knudsen diffusivity (m^2 s^{-1})
F	total molar flux (mol m^{-2} s^{-1})
F_{feed}	total molar flux of feed (mol m^{-2} s^{-1})
h_p	film heat transfer coefficient (W m^{-2} K^{-1})
h_w	wall heat transfer coefficient (W m^{-2} K^{-1})
b	adsorption equilibrium constant of component i (bar^{-1})
K_{ax}	effective axial bed thermal conductivity (W m^{-1} K^{-1})
K_{LDF}	Linear Driving Force coefficient (s^{-1})
L	length of column (m)
M	pressurization and blowdown rate parameter (s^{-1})
p_i	partial pressure of component i (barr
p	total pressure of column (bar)
q_i	adsorbed phase concentration of component i (mol kg^{-1})
$\overline{q_i}$	average adsorbed phase concentration of component i (mol kg^{-1})
q^*	equilibrium adsorbed concentration of component (mol kg^{-1})
q_m	maximum adsorbed phase concentration (mol kg^{-1})
r	particle radius (m)
r_P	pore radius (Å)
R	universal gas constant (J mol^{-1} K^{-1})
t	time (s)
T	temperature in bulk gas phase (K)
T_s	temperature in solid phase (K)
T_w	wall temperature (K)
u	superficial velocity (m s^{-1})
u_i	interstitial velocity (m s^{-1})
Y_{CO_2}	CO_2 molar fraction
y_i	molar fraction of sorbate species i in the bulk phase
z	axial coordinate in bed (m)

Subscripts/Superscripts

H	high pressure condition
L	low pressure condition

Greek letters

ΔH_i	heat adsorption of species i (J mol^{-1})
ε_b	bed porosity
ε_p	solid porosity
ρ_p	apparent adsorbent density (kg m^{-3})
τ_p	tortuosity

from Mesua ferrea L. seed cake through hydrothermal carbonization technique. They evaluated the uptake capacity of samples using breakthrough technique. Rouzitalab et al. [24] synthesized nanoporous carbon samples from walnut shell for CO_2 adsorption at the pressure range of 1-10 bar under room temperature. In a similar study, Boujibar et al. [25] considered the potential of Argan fruits shells as a source of activated carbon for carbon capture at the post-combustion operating conditions. Generally, the biomass samples (agricultural residues or waste materials) to be considered as an adsorbent in the separation processes should be physically (thermally) or chemically treated at the specified operating conditions [23,26]. In the physical treatment, the carbon samples are treated using CO_2, N_2, NH_3, or air around 600 – 900 °C, while in the chemical activation procedure different chemicals such as KOH, H_2SO_4, HCL, K_2CO_3, NaOH, H_3PO_4, or $ZnCL_2$, are employed at a temperature of less than 600 °C [23,27].

To evaluate the capacity of developed samples in the industrial scale, cyclic adsorption processes have extensively been investigated in the recent years [28]. Among different cyclic processes including Pressure/Temperature/Vacuum Swing Adsorption (PSA, TSA, VSA, …), pressure swing adsorption due to the low energy consumption has attracted much attention for CO_2 capture in the flue gases [29]. The main criterion to design a productive PSA unit is the selection of proper adsorbents compatible with post combustion operating conditions. To this end, the performance of different adsorbents has been evaluated recently [30,31]; and activated carbons because of the lower heat of adsorption introduced as an excellent candidate for cyclic adsorption processes [32].

In this work, according to the scope of CCS technology to design and develop novel processes and approaches for carbon capture and sequestration, also by considering the significance of municipal solid wastes (MSWs) management, a combination between these two global challenges has been considered. In this way, derived composts from MSWs are considered as a source of adsorbents for CO_2 capture by synthesizing five different samples using two techniques. Then, screening studies were performed in an adsorption breakthrough apparatus to find the best synthesized sample regarding CO_2 uptake. Thereafter, a mathematical model is developed to match the breakthrough curves of the best screened samples being also applied to simulate a pressure swing adsorption cycle to evaluate the capability and feasibility of the best AC sample synthesized for cyclic CO_2 purification using adsorption processes.

2. Materials and Methods

2.1. Materials and Chemicals

In this study, the compost was obtained from the urban solid waste management company (Resíduos do Nordeste, EIM, Portugal). Sulphuric acid (96–98 wt.%) was supplied by Riedel–de-Haën. Carbon dioxide and helium were furnished by Air Liquide, with purity of 99.98%, and 99.95%, respectively.

2.2. Transformation of Compost to Activated Carbon

The samples were prepared from the maturated compost and activated chemically and thermally by using sulphuric acid and calcination by N_2 flow at 400 and 800 °C, respectively. First, the materials were homogenized by mixing with water under strong stirring. Then, the raw samples were obtained by filtering the mixture. For the first sample, 3 g of the raw sample was carbonized under continuous N_2 flow (100 cm^3 min^{-1}) at 120 °C till 400 °C for 240 min (CMSW-400), while for second one (CMSW-800) the heating process continued till 800 °C. Then CMSW-S was obtained by immersing the prepared compost in 50 mL of 18 M sulphuric acid solution, for 3 h at 150 °C. To develop the fourth sample, CMSW-S was activated again in a same procedure of CMSW-800, which contributed to CMSW-S-800, while for last adsorbent (CMSW-800-S), the developed sample in the second step (CMSW-800) was chemically activated by immersing in 50 mL of 18 M sulphuric acid solution, for 3 h at 150 °C, resulted in CMSW-800-S. Finally, all samples were washed by distilled water, dried for 24 h at 110 °C and sieved to

be prepared for next step. A summary of activation procedure is illustrated in Fig. S1 (Supporting Information).

2.3. Characterization of the AC Adsorbents

The elemental composition was quantified by employing a Carlo Erba EA 1108 Elemental Analyser to determine the C, H, N and S content of the prepared samples. Thermogravimetric analysis (TGA) was performed using a Netzsch STA 409 PC equipment under oxidative atmosphere. For that purpose, the samples were heated in the air atmosphere condition from 50 to 1000 °C at 10 °C min^{-1}.

The analysis of N_2 adsorption–desorption isotherms at −196 °C was performed with a Quantachrome NOVA 4200e adsorption analyser to detect the textural properties of prepared samples. The BET specific surface area (S_{BET}) was calculated by Brunauer, Emmett, Teller method [33]. The external surface area (S_{ext}) and the micropore volume (V_{Mic}) were measured by using the *t*-method [34], and employing ASTM standard D-6556-01 to calculate the thickness (*t*). Then, the microporous surface area (S_{Mic}) was calculated by subtracting the S_{ext} from S_{BET}. Also, the approximation $W_{Mic} = 4^{V_{Mic}}/_{S_{Mic}}$ was considered to determine the average pore width (W_{Mic}). In addition, the total pore volume (V_{Total}) was considered at $^{P}/_{P0} = 0.98$.

2.4. Breakthrough Experiments (Screening Studies)

The adsorption capacities for CO_2 uptake of the prepared samples were measured using a fixed bed adsorption unit developed at LSRE-LCM. The experimental setup depicted in Fig. 1, consists in several main parts. The adsorption column containing the selected AC sample is placed inside a thermostatically controlled oven. A Thermal Conductivity Detector (TCD) measures the outlet CO_2 composition. Also, a switch valve (SV) is used to control the gas entrance flow. In addition, the gases feed flow rates are adjusted by three mass flow controllers (MFC). The pressure of the adsorption column is controlled by a Back Pressure Regulator (BPR). The helium gas is used as a carrier gas to set-up different partial pressures of CO_2. It is worth mentioning that before each experiment, the available impurity or moisture of samples were removed by passing the inert gas (Helium) in the bed of the column for 12 h at 200 °C. Thereafter, the experiments were performed by passing a constant flow rate of the mixture (carrier gas and CO_2) in the column. During the adsorption runs, the CO_2 composition was continuously measured by the TCD at the outlet of the column as a function of time. In the last step, desorption process was performed by passing pure helium through the fixed bed. More details about the unit can be found elsewhere [4,10].

Then, the dynamic equilibrium loading is obtained by integrating the molar flow profiles of the breakthrough curves using the following equation:

$$q_{exp,i} = \frac{1}{m_{ads}}\left(F_{f,i}t_n - \int_0^{t_\infty} F_i\,dt - \varepsilon_b V_c C_{i0}\right) \quad (1)$$

where m_{ads} is the adsorbent mass, $F_{f,i}$ the feed molar flow rate of component *i* at the inlet of the bed, F_i represents the molar flow rate of component *i* at the outlet of the bed, t_∞, ε_b, V_c, , are the saturation bed time, the bed porosity, the column adsorption volume, and the feed gas phase concentration at the inlet of the fixed bed, respectively.

3. Mathematical Modeling

3.1. Fixed Bed Adsorption Dynamics

Mathematical modelling and simulation of breakthrough experiments and PSA adsorption cycles is accomplished by employing the mass and energy balances on a volume element of the fixed bed column over a period of t and $t + \Delta t$. After that, the obtained set of partial differential equations (PDE'S) is solved by considering the following model assumptions [35,36]:

- The Langmuir's model is applied to describe the adsorption equilibrium.
- The flow regime is assumed as axial dispersion plug flow pattern.
- The pressure drop is negligible through the adsorption bed.
- The Linear Driving Force (LDF) model is considered for the kinetics of sorption.
- The ideal gas law is assumed.
- The system is non-isothermal non-adiabatic

Then, the breakthrough results are modelled by employing the global mass balance (Eq-1), the mass balance to the sorbate species (Eq-

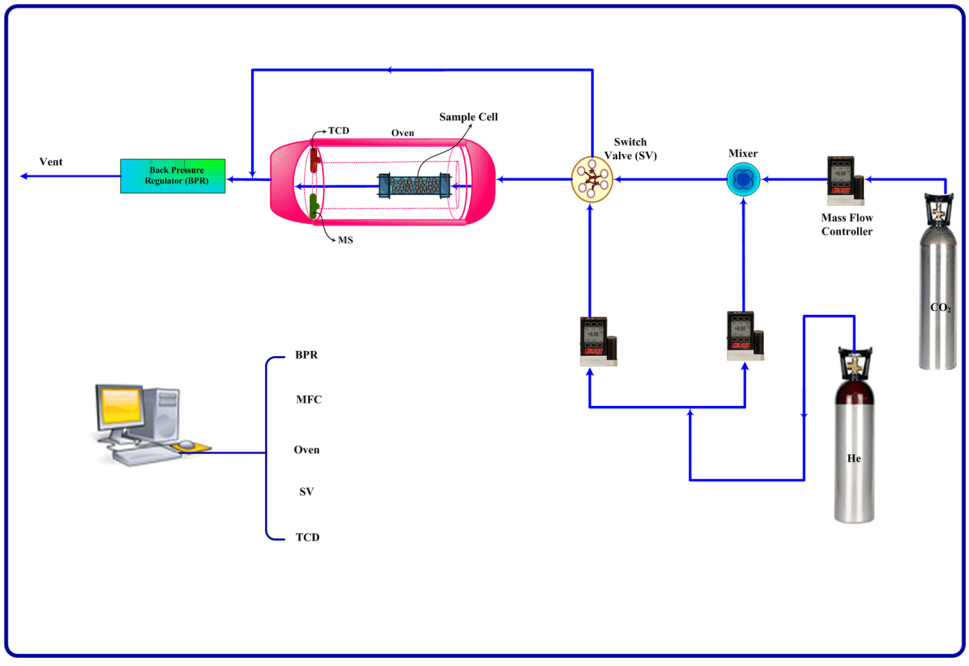

Fig. 1. The experimental set-up to evaluate the uptake capacity of prepared samples.

2), energy balance on the gas phase (Eq-3), also the energy balance on the solid phase (Eq-4). A summary of the modelling equations is shown in Table 1 . In the general mass balance equation, F, C_t, $\overline{q_i}$ and ε_b are total molar flux, total gas concentration, the average adsorbed concentration on the solid phase and the bed porosity, respectively. Also, ρ_s indicates the apparent adsorbent density, and z and t represent the axial coordinate and time, respectively. In addition, in the mass balance of sorbate species relation, D_{ax} and y_i are the axial mass dispersion coefficient and the molar fraction of the solute in the bulk phase, respectively. Furthermore, it should be considered that the mass transfer rate from the bulk gas to the adsorbent particles has been considered as a linear model, which is calculated by the linear driving force (LDF) Eq-6 [35], here $q*$ and $\overline{q_i}$ are the concentration of the adsorbed phase in equilibrium with bulk gas, and the average adsorbed phase concentration of species i in the solid sorbents, respectively.

On the other hand, as can be observed in Table 1, the energy balance on the gas phase is calculated by Eq-3, where T_s is the solid phase temperature and T_w the wall temperature, also K_{ax}, c_{pg}, h_f and h_w represent the axial bed thermal conductivity, the heat capacity of the gas phase, the heat transfer coefficient of the film, and the overall heat transfer coefficient, respectively. In addition, the energy balance on the solid phase is calculated by Eq-4. Here c_{ps} is the heat capacity of the solid adsorbent, and $(-\Delta H_i)$ the heat of adsorption.

3.2. Pressure Swing Adsorption Design

In this work, a PSA cycle was designed and simulated by using the best sample of AC derived from the CMSW for purification purposes. The cycle comprises typical four main steps including: i) pressurization with feed, ii) feed at high-pressure, iii) co-current depressurization, and iv) counter-current purge [37,38]. The considered boundary conditions to design the system of partial differential equations are presented in Table 2 . In this way, the designed PSA cyclic process was scaled up to treat a feed gas containing the CO_2 as an impurity.

3.3. Numerical Simulation of Mathematical Model

The set of partial differential equations (PDEs) arising from the governing equations and auxiliary relations for the mathematical modeling of the adsorption process can be simplified into a set of ordinary differential equations (ODEs) and solved by a proper numerical technique. One of the most popular strategies is the method of lines (MOL). This strategy is a semi-discrete method, which discretizes the spatial variables by keeping the time parameter [39,40]. Then, the space partial derivatives were algebraically approximated by finite differences using the *dss* routines and the resulting system is integrated as a function of time with the stiff integrator, ode 15 s, in MATLAB code.

4. Results and Discussion

4.1. Characterization of Adsorbents

The elemental analysis of prepared samples has been reported in Table 3 . As can be observed, ashes content in all samples, which was measured by TGA, is higher than other elements (C, H, S and N) also the carbon content is less than 25% for all samples (15.6%, 17.5%, 20.1%, 20.5% and 18.5% for CMSW-400, CMSW-800, CMSW-S, CMSW-S-800 and CMSW-800-S, respectively), which is a typical behaviour in the biochar carbon materials [41,42]. Also, CMSW-800, CMSW-S-800 and CMSW-800-S, which have been treated at 800 ˚C have the higher percentage of ashes (80.6%, 65.9% and 72.4%, respectively) than other ones. In addition, as can be expected, CMSW-S has the lowest ashes percentage (34.3%) which can be ascribed to the removal of the inorganic content with acid, as well as, this sample shows higher difference between non-CHSN and ashes content likely due to the oxidation of the materials by the acid attack. The calcination and acid treatments contributed to the burn-off (weight loss) in consonance with the disappearance of volatile compounds and inorganic substances as consequence of the calcination and acid treatments, respectively. These mass losses resulted in the development of the porosity for each sample, which as can be observed by the nitrogen adsorption-desorption isotherms at −196 ˚C on the prepared adsorbents (Fig. 2).

As shown, the N_2 adsorption at −196 ˚C of the prepared samples can be considered as isotherm type II with a hysteresis loop, based on the the last classification of physisorption isotherms of the IUPAC, which the hysteresis loop can also be classified as H3, typically found for this type of isotherms. On the other hand, BET and *t*-plot methods were employed to obtain the textural properties of the samples. As can be observed in Table 4, different treatments contributed to develop higher specific surface. Among all samples, CMSW-S-800 shows the highest surface area than other ones, which can be ascribed to the thermal treatment of this sample after the chemical activation. In this way, some of the functional groups that are able to block the available pores, were removed and some new adsorption sites emerged. Thus, this sample represents apparently the better performance for CO_2 uptake.

4.2. Screening Studies Regarding CO_2 Uptake

At the first step, several breakthrough runs were performed to evaluate the adsorption capacity of the synthesized samples in terms of their adsorption capacities for detecting the best samples. The breakthrough tests were accomplished at 40, 70 and 100 ˚C and in the pressure range of 1-5 bar. A comparison between fixed bed breakthrough curves of all AC samples at 40 ˚C and 2.5 bar is shown in Fig. 3,

Table 1
Mass and energy balances and respective initial and boundary conditions for mathematical modeling of breakthrough experiments.

Equations:	Boundary and Initial Conditions:	
Total mass balance: $\frac{\partial F}{\partial z} + \varepsilon_b \frac{\partial C_t}{\partial t} + (1-\varepsilon_b)\rho_s \sum_{i=1}^{n} \frac{\partial \overline{q_i}}{\partial t} = 0$	$Z = 0;\ t\rangle 0;\ F = F_f$ $t = 0,\ \forall\ z;\ \overline{q_i} = 0;\ F = F_f;\ C = C_f$	(2)
Mass balance to sorbate species: $-\varepsilon_b D_{ax} \frac{\partial}{\partial Z}(C_t \frac{\partial y_i}{\partial z}) + \frac{\partial (F y_i)}{\partial z} + \varepsilon_b \frac{\partial (C_t y_i)}{\partial t} + \rho_s (1-\varepsilon_b) \frac{\partial \overline{q_i}}{\partial t} = 0$	$t = 0,\ \forall\ z;\ y = \overline{q_i} = 0$ $Z = 0;\ t\rangle 0;\ F y_{if} = F y_i - \varepsilon_b D_{ax} C \frac{\partial y_i}{\partial z}$ $z = l;\ t\rangle 0;\ \frac{\partial y_i}{\partial z} = 0$	(3)
Energy balance on the gas phase: $-K_{ax} \frac{\partial 2T}{\partial z2} + F c_{pg} \frac{\partial T}{\partial z} + \varepsilon_b C_t c_{pg} \frac{\partial T}{\partial t} + (1-\varepsilon_b) a_p h_f (T - T_S) + a_c h_w (T - T_w) = 0$	$z = 0;\ t\rangle 0;\ F c_{pg} T_f = F c_{pg} T - K_{ax} \frac{\partial T}{\partial z}$ $z = l;\ t\rangle 0;\ \frac{\partial T}{\partial z} = 0$ $t = 0,\ \forall\ z;\ T = T_s = T_f$	(4)
Energy balance on the solid phase: $c_{ps} \frac{\partial T_S}{\partial t} = a_p h_p (T - T_s) + \sum_{i=1}^{n} (-\Delta H_i) \frac{\partial \overline{q_i}}{\partial t}$		(5)
Kinetics of sorption: $\frac{\partial \overline{q_i}}{\partial t} = k_{LDF} (q^* - \overline{q_i})$		(6)

Table 2
The considered boundary conditions for designing the PSA unit.

Step I	Pressurization with Feed	$P = (P_H - P_L)[1 - \exp(-Mt)] + P_L$ $z = 0$: $F = F_H$ $\varepsilon_b D_{ax}\rho\frac{\partial y_i}{\partial z} = F(y_i - y_{iH})$ $K_{ax}\frac{\partial T}{\partial z} = FC_{pg}(T - T_H)$	$z = L$: $F = 0$ $\frac{\partial y_i}{\partial z} = 0$ $\frac{\partial T}{\partial z} = 0$
Step II	High Pressure Feed	$P = P_H$ $z = 0$: $F = F_H$ $\varepsilon_b D_{ax}\rho\frac{\partial y_i}{\partial z} = F(y_i - y_{iH})$ $K_{ax}\frac{\partial T}{\partial z} = FC_{pg}(T - T_H)$	$z = l$ $\frac{\partial y_i}{\partial z} = 0$ $\frac{\partial T}{\partial z} = 0$
Step III	Co-current Depressurization	$P = (P_H - P_L)[\exp(-Mt)] + P_L$ $z = 0$: $F = F_H$ $\varepsilon_b D_{ax}\rho\frac{\partial y_i}{\partial z} = F(y_i - y_{iH})$ $K_{ax}\frac{\partial T}{\partial z} = FC_{pg}(T - T_H)$	$z = l$ $\frac{\partial y_i}{\partial z} = 0$ $\frac{\partial T}{\partial z} = 0$
Step IV	Counter Current Low Pressure Purge	$P = P_L$ $z = 0$ $\frac{\partial y_i}{\partial z} = 0$ $\frac{\partial T}{\partial z} = 0$	$z = L$: $F = F_L$ $\varepsilon_b D_{ax}\rho\frac{\partial y_i}{\partial z} = F(y_{iL} - y_i)$ $K_{ax}\frac{\partial T}{\partial z} = FC_{pg}(T_L - T)$

Table 3
Elemental analysis of the prepared samples.

Sample	C (%)	H (%)	S (%)	N (%)	Remaining* (%)	Ashes$^{\Psi}$ (%)
CMSW-400	15.6	1.0	0.3	0.9	82.2	64.9
CMSW-800	17.5	0.4	0.4	0.0	81.6	80.6
CMSW-S	20.1	2.3	0.6	1.7	70.4	34.3
CMSW-S-800	20.5	1.9	0.4	1.4	75.8	65.9
CMSW-800-S	18.6	0.5	8.1	0.0	72.7	72.4

* Remaining was obtained from the subtraction of C, H, S, N content from 100%.

$^{\Psi}$ Ashes values corresponds with the weight of the samples at the end of the TGA in oxidizing atmosphere.

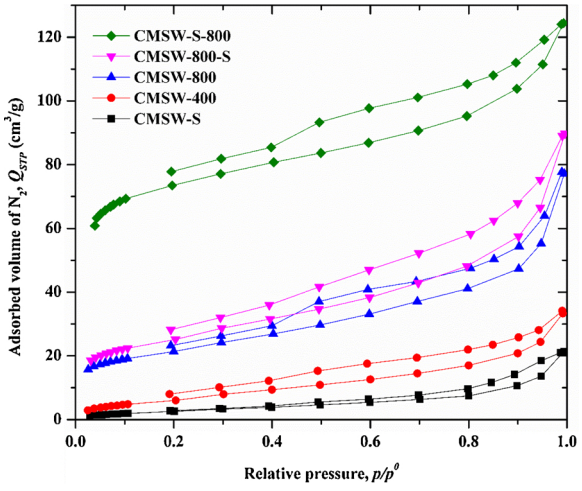

Fig. 2. Adsorption Isotherms (adsorption-desorption branch) of nitrogen at −196 °C on prepared AC samples.

also details of other runs can be found in Supporting Information (Fig. S2-S5 and Tables S1-S4). As can be observed in Fig. 3, CMSW-S-800, which has been firstly treated with sulfuric acid, then thermally activated at 800 °C, has the highest breakthrough time (around 3.5 min) than other ones, and consequently (as shown in Fig. 3b) this sample has the highest uptake capacity. The difference in the breakthrough time between the best (CMSW-S-800) and worst (CMSW-400) samples is around 1 min (practically the double). Also from Fig. 3a it can be retained that the mass transfer zone of the breakthrough curves is very narrow, which indicates adsorption kinetic is very rapid in the synthesized AC´s. Fig. 3b represents that the loading capacity for CO_2 (calculated from the integration of the breakthrough profiles Eq. 1) for CMSW-S-800 sample is around 2.5 mmol/g and for CMSW-400 sample only 1 mmol/g.

Table 4
Burn-off during the preparation of the prepared samples and textural properties of materials determined from BET and *t*-plot methods.

Sample	Burn-off (%)	S_{BET} ($m^2 \cdot g^{-1}$)	S_{ext} ($m^2 \cdot g^{-1}$)	S_{mic} ($m^2 \cdot g^{-1}$)	V_{mic} ($mm^3 \cdot g^{-1}$)	V_{mic}/V_{Total} (%)	W_{mic} (nm)
CMSW-400	23.9	22	22	0	0	0.0	0.0
CMSW-800	39.9	77	52	25	12	14.0	1.9
CMSW-S	59.6	11	11	0	0	0.0	-
CMSW-S-800	76.3	279	56	223	92	53.4	1.6
CMSW-800-S	58.7	91	60	31	14	13.6	1.8

4.3. Adsorption Equilibrium Isotherms of CO_2

The dynamic method to study the adsorption equilibrium means that one fixed bed experiment represents a single point for the measurements of the adsorption equilibrium isotherm. The measured uptake capacities from the breakthrough technique for all samples at 40 °C are represented in Fig. 4, resulting in the respective adsorption equilibrium isotherms. The adsorption isotherms illustrated in Fig. 4a show the CMSW-S-800 sample has an uptake capacity of 2.5 mmol/g at 2.5 bar and 40 °C (around 11% (wt%)) and the CMSW-400 and CMSW-800 demonstrate the lowest adsorption capacities (below 1 mmol/g) at a similar pressure and temperature (2.5 bar and 40 °C), which it can be interpreted based on several factors. First, it should be considered that the chemical activation is the dominant agent on the activation of the carbon based materials than thermal activation [43], thus the CMSW-400 and CMSW-800, which were just thermally treated at 400 and 800 °C, respectively, have the lowest uptake capacities than other ones. On the other hand, the higher uptake capacity of CMSW-S-800 can be ascribed to the microporosity quality of this sample, as main character of carbon based materials for CO_2 adsorption [4], which due to the thermal activation of this sample after chemical treatment, oxygen groups (SOGs), that play an important role in the adsorption process, are discharged by releasing CO and CO_2 components [44,45]. Thus, based on the thermal treatment of this sample, it can be accepted that most of SOGs are desorbed and concluded the CMSW-S-800 material

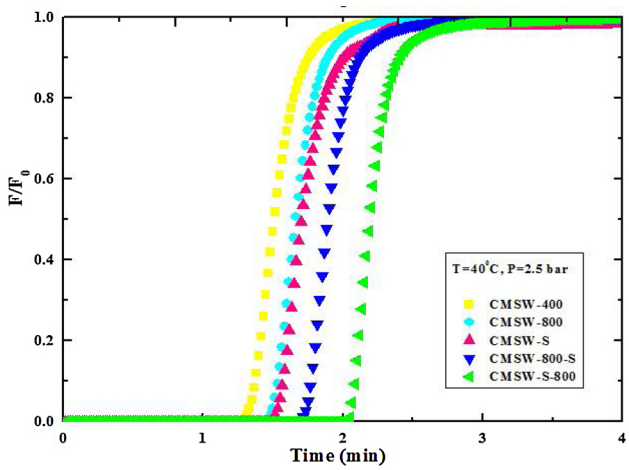

a

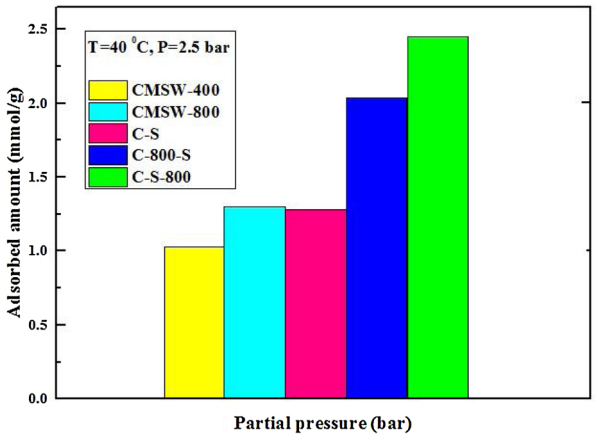

b

Fig. 3. (a) Screened breakthrough curves and (b) respective uptake capacities of synthesized AC samples at 40 °C and 2.5 bar.

with a better surface chemistry accompanied with more active sites for CO_2 adsorption [46].

A comparison between the isotherms of CMSW-800-S and CMSW-S-800 (as the best obtained samples) was also performed at different temperatures (Figs. 4 b & c). As can be expected, based on the exothermic nature of the adsorption process, the uptake capacities are reduced by increasing the temperature. On the other hand, by increasing the pressure, the uptake capacities of samples raise in all considered temperatures, due to the increment of thermodynamic driving force. It is worth mentioning that the adsorption equilibrium results have been accomplished by using the Langmuir isotherm, which is defined by:

$$q_e = \frac{q_m b P_{CO_2}}{1 + b P_{CO_2}} \tag{6}$$

here q_e, q_m and P_{CO_2} are the adsorption capacity at equilibrium conditions, the maximum adsorption capacity and the partial pressure of CO_2, respectively. Also, b represents the Langmuir equilibrium adsorption constant. As can be observed, Langmuir model can describe very well the adsorption equilibrium data. Also, small curvatures in Fig. 4 b and c are another interesting feature of the presented

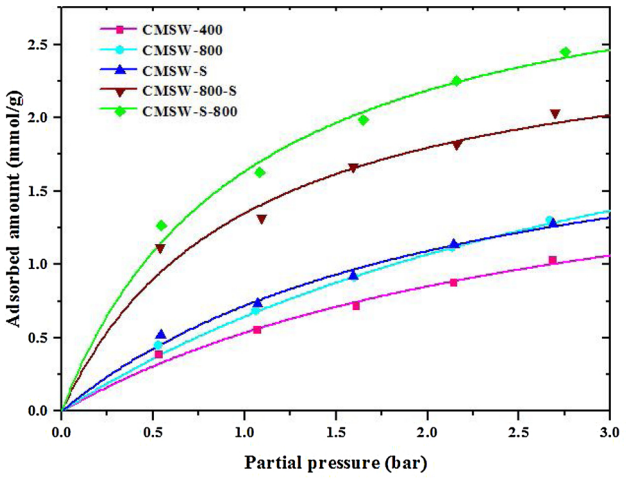

a

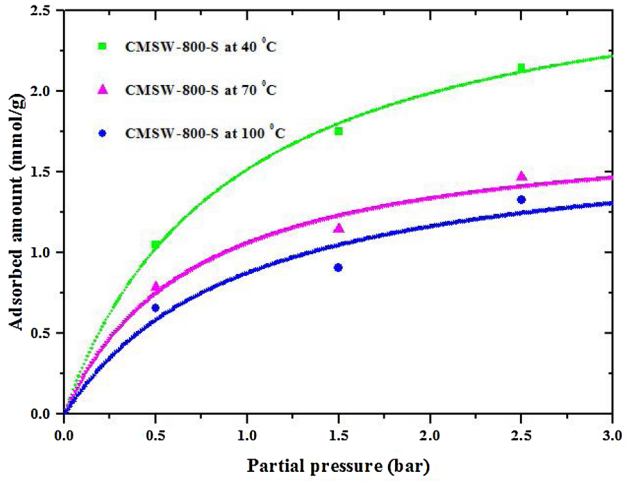

b

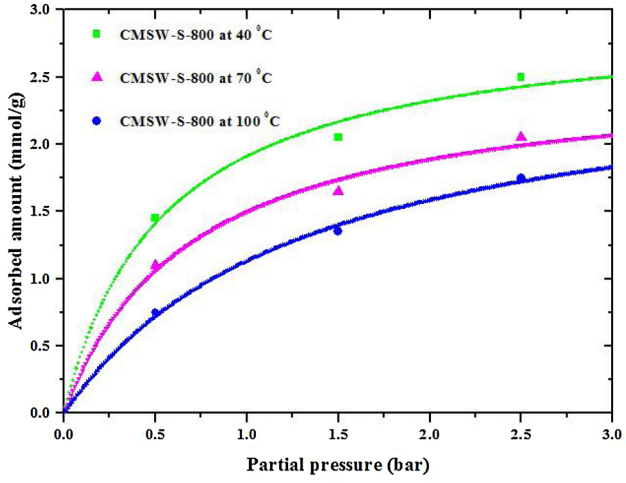

c

Fig. 4. Comparison of adsorption equilibrium isotherms of (a) all samples at 40 °C and (b) CMSW-800-S and (c) CMSW-S-800 and at 70 and 100 °C.

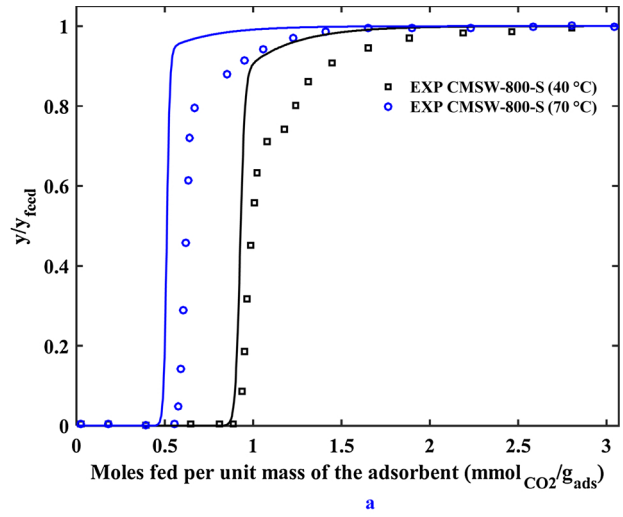

a

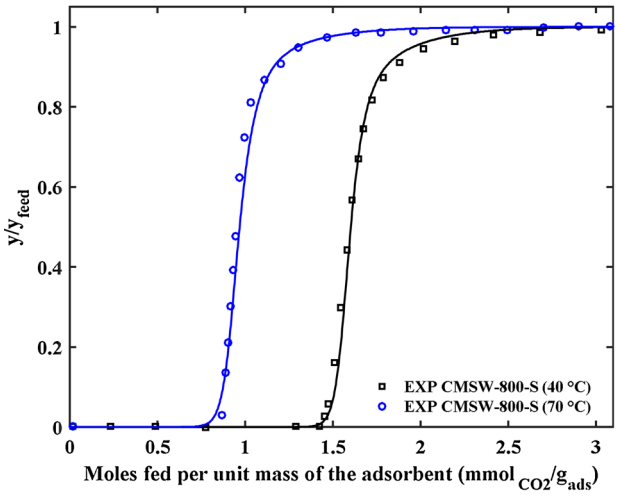

b

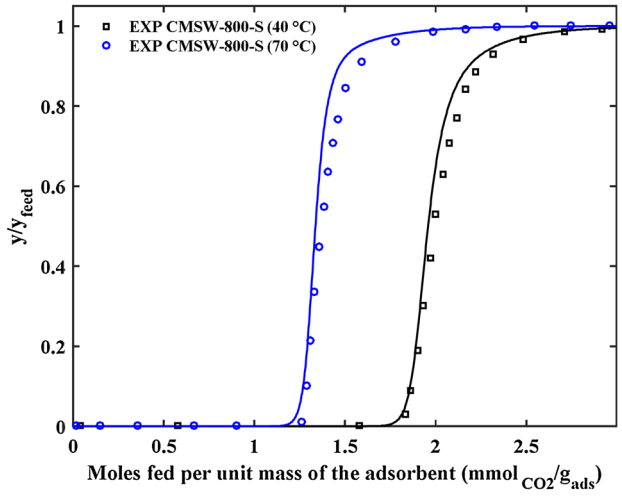

c

Fig. 5. Breakthrough adsorption curves plotted in terms of the normalized concentration of concentration of CO_2 as a function of moles fed per unit mass of adsorbent for RUNs in CMSW-800-S sample at 40 and 70 ˚C and total pressure: (a) 1 bar, (b) 3 bar (c) 5 bar. Points are experimental data and lines model predictions.

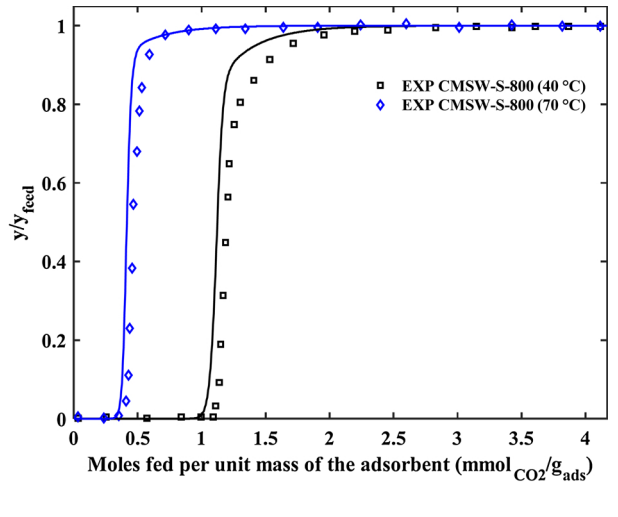

a

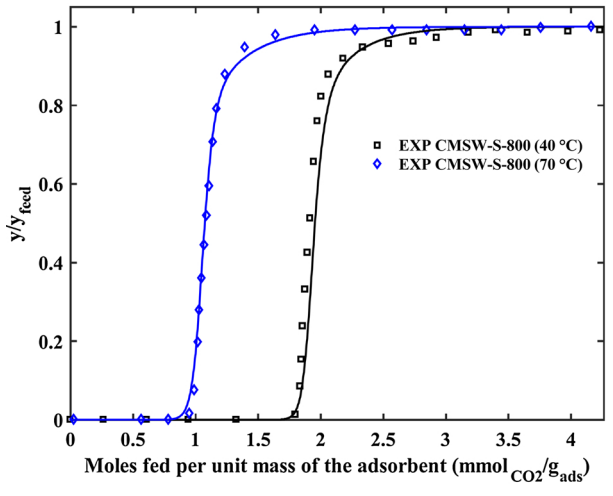

b

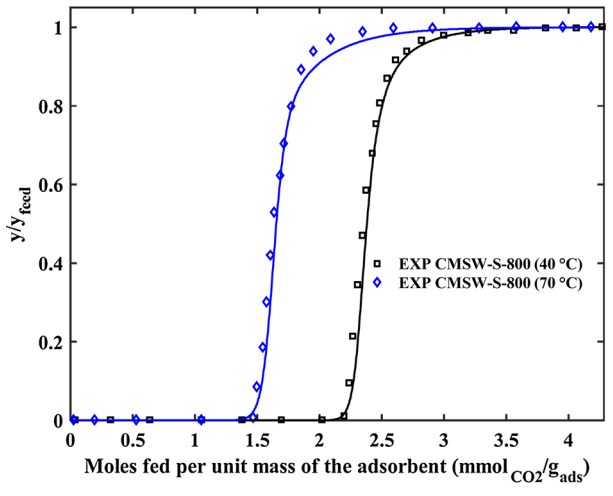

c

Fig. 6. Breakthrough adsorption curves plotted in terms of the normalized concentration of concentration of CO_2 as a function of moles fed per unit mass of adsorbent for RUNs in samples CMSW-S-800 at 40 and 70 ˚C and total pressure: (a) 1 bar, (b) 3 bar (c) 5 bar. Points are experimental data and lines model predictions.

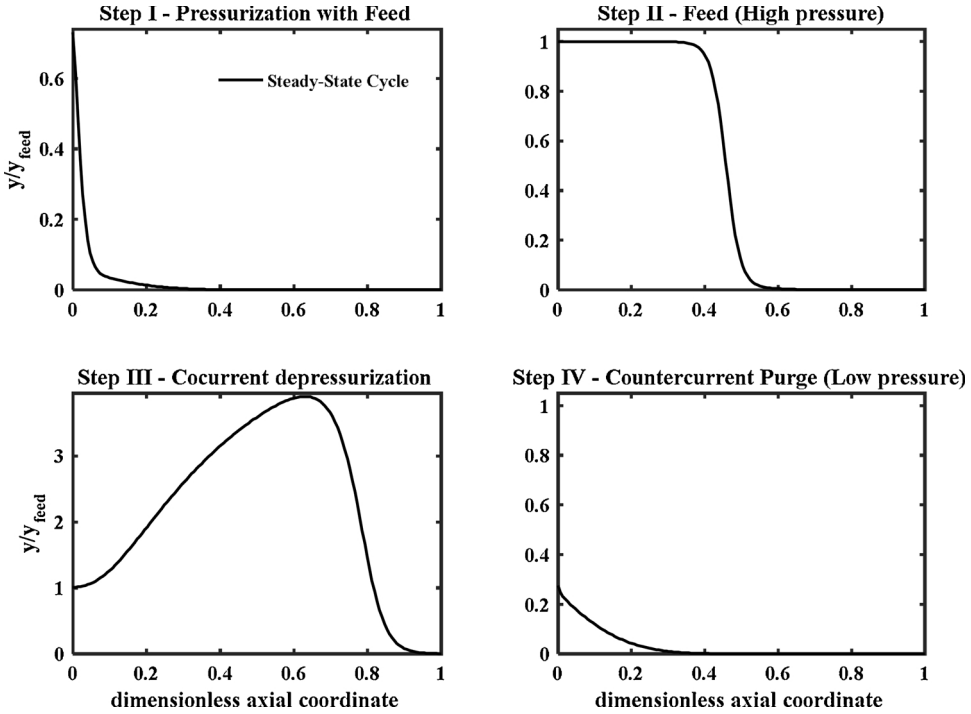

Fig. 7. Axial molar fraction profiles of carbon dioxide at the end of the four steps of the PSA (at cyclic steady state). (Operating conditions are shown in Table 6).

Table 5
Operating conditions and model parameters of breakthrough runs for CMSW-800-S and CMSW-S-800 samples at 40 °C.

Parameter	CMSW-S-800			CMSW-800-S		
Pressure	1 bar	3 bar	5 bar	1 bar	3 bar	5 bar
Operating conditions						
$F_{feed}(mol\,m{-}2s{-}1)$	0.85	0.85	0.85	0.85	0.85	0.85
T (K)	313	313	313	313	313	313
y_{CO_2}	0.55	0.55	0.55	0.55	0.55	0.55
y_{He}	0.45	0.45	0.45	0.45	0.45	0.45
Model parameters						
$K_{ax}(W\,m{-}1K{-}1)$[a]	0.057	0.019	0.012	0.058	0.019	0.012
$h_P(W\,m{-}2K{-}1)$[b]	1384	461	275	1376	445	274
$h_W(W\,m{-}2K{-}1)$	39			39		
$C_{pg}(J\,g{-}1K{-}1)$	1.17			1.17		
$C_{ps}(J\,g{-}1K{-}1)$[c]	1.36			1.36		
Pem [d]	90			90		
$K_{LDF}(s{-}1)$	0.25	0.25	0.25	0.33	0.30	0.30
Bed and adsorbent properties						
bed length $L(m)$	0.081					
bed diameter $d_b(m)$	0.0044					
bed porosity ε_b	0.4					
Avg adsorbent diameter $d_a(m)$	$1.1 \times 10{-}4$					
mass of adsorbent $m_a(g)$	0.41		0.40			
feed temperature, $T(K)$	313		313			
Isotherm parameters						
$q_m(mol\,kg{-}1)$	3.29		2.68			
$b\,(bar{-}1)$ at 313 K	0.985		1.01			
$\Delta H\,(kj\,mol{-}1)$	−21.6		−20.4			

[a] Effective axial bed thermal conductivity, K_{ax}, was estimated by the correlation $K_{ax} = C_f D_{ax}$, taking from Ruthven (C_f is the gaseous heat capacity) [1].

[b] The film heat transfer was estimated from the limit of Nusselt number, $Nu = \frac{2R_p h_p}{\lambda_f} \approx 2.0$, $\lambda_f = C_f D_{AB}$, taken from Ruthven [35].

[c] Heat capacity of solid was calculated from correlation available in Poling [47].

[d] The Peclet number was estimated by $Pem = v_i L/D_{ax}$, being D_{ax} calculated by the correlation $D_{ax} = 0.7D_m + 0.5d_p v_i$, taken from Ruthven [35].

equilibrium data, which is one of the main benefits for developing cyclic adsorption processes, especially for the regeneration step to reduce the energy consumption.

4.4. Breakthrough Modeling

The breakthrough results of the best samples CMSW-800-S and CMSW-S-800 are depicted in Figs. 5 and 7 to evaluate the impact of temperature and pressure on the CO_2 capture, respectively. Also, the outcomes of other runs are reported in the Supporting Information (Fig. S2-S5 and Tables S1-S4). It is worth mentioning that Figs. 5 & 6 are represented in terms of the normalized concentration of CO_2 as a function of the amount of moles fed per unit mass of adsorbent for a direct comparison between the CO_2 uptake capacity (points are experimental data and lines represent model predictions). In addition, the breakthrough curves as a function of time are reported in the Supporting Information (Figures S3-S5). It should be considered that the parameters of the mathematical model considered for the model predictions of the experimental data were obtained from available correlations on literature (Dax, Kax, hp, Cpg; hw) [35,47]. In this way, the K_{LDF} parameter (mass transfer coefficient) is the only one that should be considered in the mathematical model to match the experimental breakthrough curves. The values of K_{LDF} (for best match of experimental breakthrough runs) are reported In Table 5, which were obtained by a trial and error procedure.

As can be observed in Figs. 5 and 6, in all runs, as expected, the breakthrough uptake capacity enhances by increasing the pressure. Also, for the same sample at the same pressure, because of the exothermic nature of the adsorption process, the breakthrough uptake capacity reduces by increasing the temperature. As shown, there is a good agreement between the experimental data and modeling results in all runs. Concerning the model parameters, it should be considered that the mass transfer zone of the breakthrough curves is very sharp at the outlet of the bed. It illustrates that there is not significant mass transfer resistances for spreading zone. In addition, the Peclet number that represents the axial dispersion is high in the bed with values around 90. These fixed bed adsorption results, demonstrate that the best sample of AC´s synthesized from the CMSW, has a low mass transfer resistance for

Table 6
Model parameters, operating conditions and considered time of each step of the simulated PSA cycle.

Parameter	Value	
Bed and adsorbent properties		
bed length $L\,(m)$	5	
bed diameter $d_b(m)$	1.62	
bed porosity ε_b	0.4	
avg adsorbent diameter $d_a(m)$	$1.1 \times 10{-}4$	
mass of adsorbent $m_a(g)$	3442	
bed density $\rho_b(kg\,m{-}3)$	333	
feed temperature $T\,(K)$	313	
Isotherm parameters		
$q_m\,(mol\,kg{-}1)$	3.3	
$b\,(bar{-}1)$ at 313 K	0.985	
Operating conditions	High	Low
$F\,(mol\,m{-}2s{-}1)$	16.84	13.47
$T\,(K)$	313	313
$P\,(bar)$	5	1
y_{CO_2}	0.088	0
Inert	0.912	1
Pe	90	90
$K_{LDF}\,(s{-}1)$	0.25	0.25
Time of each step		
pressurization with feed,(min)	0.5	
high-pressure feed, (min)	8.5	
Co-current blow down, (min)	1	
Countercurrent low pressure purge, (min)	6	

CO_2 adsorption, which is a benefit to be used in cyclic adsorption processes, and improve the cyclic adsorption processes, by decreasing the width of the mass transfer zones and therefore reducing the length of the unused bed (LUB).

4.5. Simulation of a Pressure Swing Adsorption Cycle for the Best AC sample

To obtain a feedback concerning the application of the best synthesized CMSW in a cyclic PSA adsorption processes, simulations were performed to develop an insight about its application to remove CO_2 from a gas stream. According to the described cycle in section 3 (Mathematical Modeling), the main steps of the simulated PSA cycle include: i) pressurization with feed, ii) feed at high-pressure, iii) co-current depressurization, and iv) countercurrent purge with an inert. In Table 6, the model parameters, for the operating conditions of the developed PSA cycle, and also the considered time of each step are reported.

Fig. 7 shows the axial molar profile of the CO_2 at the end of the four cycles at the cyclic steady-state, for the reported operating conditions in Table 6. As can be observed, at the end of the co-current blow-down (step iii), only a small fraction of the bed is free of sorbate (CO_2) (which illustrates an efficient usage of the bed). In addition, in the countercurrent purge (step IV), the molar fraction of the carbon dioxide in the gas phase is reduced to a very small value, that proves the bed is efficiently regenerated. This can be ascribed to the synthesized AC material that resulted in isotherms with a small type I curvature (which is beneficial for cleaning the adsorption columns), and also a high mass transfer rate with no significant mass transfer resistances. The data shown in Figure 8 represents that AC´s derived from MSWC can be successfully employed to remove CO_2 from flue gas using PSA cyclic adsorption processes.

5. Conclusion

The potential of derived compost from municipal solid wastes for purification of CO_2 was investigated in the present work. In this way, five different samples were treated by sulfuric acid and activated by N_2 at 400 and 800 ˚C. The equilibrium adsorptions of samples were measured by a dynamic fixed bed breakthrough technique. The results revealed that the CMSW-S-800 material, which was firstly treated with sulfuric acid, then activated at 800 ˚C was the best sample, with an uptake capacity around 2.6 mmol/g at 40 ˚C and 3 bar, which is in the range of commercial carbon materials. Thereafter a mathematical model has been calibrated to simulate the fixed bed adsorption data, with parameters calculated from correlations available on literature. The match of the breakthrough profiles showed that mass transfer in the best AC sample is fast. Finally, a PSA unit was designed to evaluate the performance and capacity of best prepared sample for CO_2 removal in a flow stream mixed with an inert. Results showed an efficient removal of CO_2 and regeneration of the bed. Finally, this work reveals that the derived compost from municipal solid wastes can be considered as a low cost adsorbent for CO_2 adsorption giving a possible different end to this problematic residue.

6. Credit Author Statement

All persons who meet authorship criteria are listed as authors, and all authors certify that they have participated in the work to take public responsibility for the content, including participation in the concept, design, analysis, writing, or revision of the manuscript. Furthermore, each author certifies that this material or similar material has not been and will not be submitted to or published in any other publication before its appearance in the Journal of Environmental Chemical Engineering.

Declaration of Competing Interest

The authors declare that they have no known competing financial interests or personal relationships that could have appeared to influence the work reported in this paper.

Acknowledgment

This work was financially supported by: Project POCI-01-0145-FEDER-006984 – Associate Laboratory LSRE-LCM funded by FEDER through COMPETE2020 Programa Operacional Competitividade e Internacionalização (POCI) and project “VALORCOMP" (ref.0119_VALORCOMP_2_P), financed through INTERREG V A Spain Portugal (POCTEP) 2014-2020 –by national funds through FCT, and Project NORTE-01-0145- FEDER-000006, supported by Norte’s Regional Operational Programme (NORTE 2020), under the Portugal 2020 Partnership Agreement, through the European Regional Development Fund, also it received financially support from CIMO under UID/AGR/00690/2019. M. Karimi acknowledges PhD research grant awarded under Project: SFRH/BD/140550/2018 by Foundation for Science and Technology (FCT, Portugal). In addition, Authors would like to appreciate Prof. Helder T. Gomes and Dr. Jose L. Diaz de Tuesta from CIMO for their collaboration in VALORCOMP project.

Appendix A. Supplementary data

Supplementary material related to this article can be found, in the online version, at doi:https://doi.org/10.1016/j.jece.2020.104069.

References

[1] F.T. Tangang, J. Liew, E. Salimun, M.S. Kwan, J.L. Loh, H. Muhamad, Climate change and variability over Malaysia: Gaps in science and research information, Sains Malays. 41 (2012) 1355–1366.
[2] C. Goel, H. Bhunia, P.K. Bajpai, Novel nitrogen enriched porous carbon adsorbents for CO2 capture: Breakthrough adsorption study, J. Environ. Chem. Eng. 4 (2016) 346–356.
[3] R.L. Siegelman, P.J. Milner, E.J. Kim, S.C. Weston, J.R. Long, Challenges and

opportunities for adsorption-based CO2 capture from natural gas combined cycle emissions, Energy Environ. Sci. 12 (2019) 2161–2173.
[4] M. Karimi, J.A.C. Silva, C.N.d.P. Gonçalves, J.L. Diaz de Tuesta, A.E. Rodrigues, H.T. Gomes, CO2 capture in chemically and thermally modified activated carbons using breakthrough measurements: experimental and modeling study, Ind. Eng. Chem. Res. 57 (2018) 11154–11166.
[5] N.A. Rashidi, S. Yusup, A. Borhan, Isotherm and thermodynamic analysis of carbon dioxide on activated carbon, Procedia Eng. 148 (2016) 630–637.
[6] N. Mac Dowell, P.S. Fennell, N. Shah, G.C. Maitland, The role of CO2 capture and utilization in mitigating climate change, Nat. Clim. Change. 7 (2017) 243–249.
[7] Z. Wang, L. Zhan, M. Ge, F. Xie, Y. Wang, W. Qiao, X. Liang, L. Ling, Pith based spherical activated carbon for CO2 removal from flue gases, Chem. Eng. Sci. 66 (2011) 5504–5511.
[8] A. Kongnoo, P. Intharapat, P. Worathanakul, C. Phalakornkule, Diethanolamine impregnated palm shell activated carbon for CO2 adsorption at elevated temperatures, J. Environ. Chem. Eng. 4 (2016) 73–81.
[9] W. Li, K. Goh, C.Y. Chuah, T.H. Bae, Mixed-matrix carbon molecular sieve membranes using hierarchical zeolite: A simple approach towards high CO2 permeability enhancements, J. Membrane Sci. 588 (2019) 117220.
[10] A. Henrique, M. Karimi, J.A.C. Silva, A.E. Rodrigues, Analyses of adsorption behavior of CO2, CH4, and N2 on different types of BETA zeolites, Chem. Eng. Technol. 42 (2019) 327–342.
[11] J. Yu, Y. Wu, P.B. Balbuena, Response of metal sites toward water effects on post-combustion CO2 Capture in metal–organic frameworks, ACS Sustainable Chem. Eng. 4 (2016) 2387–2394.
[12] X. Song, M. Zhang, C. Chen, J. Duan, W. Zhang, Y. Pan, J. Bai, Pure-supramolecular-linker approach to highly connected metal–organic frameworks for CO2 capture, J. Am. Chem. Soc. 141 (2019) 14539–14543.
[13] A. Sanna, M.M. Maroto-Valer, CO2 capture at high temperature using fly ash-derived sodium silicates, Ind. Eng. Chem. Res. 55 (2016) 4080–4088.
[14] D.V. Quang, A. Dindi, M.R.M. Abu-Zahra, One step process using CO2 for the preparation of amino-functionalized mesoporous silica for CO2 capture application, ACS Sustainable Chem. Eng. 5 (2017) 3170–3178.
[15] M. Fattahi, M. Kazemeini, F. Khorasheh, A.M. Rashidi, Vanadium pentoxide catalyst over carbon-based nanomaterials for the oxidative dehydrogenation of propane, Ind. Eng. Chem. Res. 52 (2013) 16128–16141.
[16] M. Pardakhti, T. Jafari, Z. Tobin, B. Dutta, E. Moharreri, N.S. Shemshaki, S. Suib, R. Srivastava, Trends in solid adsorbent materials development for CO2 capture, ACS Appl. Mater. Interfaces 11 (2019) 34533–34559.
[17] M.F. Hassan, M.A. Sabri, H. Fazal, N. Shezad, M. Hussain, A. Hafeez, Recent trends in activated carbon fibers production from various precursors and applications—A comparative review, J. Anal. Appl. Pyrol. 145 (2020) 104715.
[18] S. García, M.V. Gil, C.F. Martín, J.J. Pis, F. Rubiera, C. Pevida, Breakthrough adsorption study of a commercial activated carbon for pre-combustion CO2 capture, Chem. Eng. J. 171 (2011) 549–556.
[19] H. Yu, X. Wang, C. Xu, D.L. Chen, W. Zhu, R. Krishna, Utilizing transient breakthroughs for evaluating the potential of Kureha carbon for CO2 capture, Chem. Eng. J. 269 (2015) 135–147.
[20] S. Choi, J.H. Drese, C.W. Jones, Adsorbent materials for carbon dioxide capture from large anthropogenic point sources, ChemSusChem 2 (2009) 796–854.
[21] J. Wang, Y. Yang, Q. Jia, Y. Shi, Q. Guan, N. Yang, P. Ning, Q. Wang, A critical review on solid waste derived CO2 capturing materials, ChemSusChem 12 (2019) 2055–2082.
[22] A.A. Azmi, M.A.A. Aziz, Mesoporous adsorbent for CO2 capture application under mild condition: A review, J. Environ. Chem. Eng 7 (2019) 103022.
[23] L.K.G. Bhatta, S. Subramanyam, M.D. Chengala, U.M. Bhatta, N. Pandit, K. Venkatesh, Investigation of CO2 adsorption on carbon material derived from Mesua ferrea L. seed cake, J. Environ. Chem. Eng. 3 (2015) 2957–2965.
[24] Z. Rouzitalab, D.M. Maklavany, A. Rashidi, S. Jafarinejad, Synthesis of N-doped nanoporous carbon from walnut shell for enhancing CO2 adsorption capacity and separation, J. Environ. Chem. Eng. 6 (2018) 6653–6663.
[25] O. Boujibar, A. Souikny, F. Ghamouss, O. Achak, M. Dahbi, T. Chafik, CO2 capture using N-containing nanoporous activated carbon obtained from Argan fruit shells, J. Environ. Chem. Eng. 6 (2018) 1995–2002.
[26] M. Olivares-Marín, M. Maroto-Valer, Development of adsorbents for CO2 capture from waste materials: a review, Greenhouse Gas Sci Technol. 2 (2012) 20–35.
[27] T. Tay, S. Ucar, S. Karagoz, Preparation and characterization of activated carbon from waste biomass, J Hazard Mater 165 (2009) 481–485.
[28] I. Durán, F. Rubiera, C. Pevida, Vacuum swing CO2 adsorption cycles in waste-to-energy plants, Chem. Eng. J. 382 (2020) 122841.
[29] S. Sircar, Pressure Swing Adsorption, Ind. Eng. Chem. Res. 41 (2002) 1389–1392.
[30] R.L.S. Canevesi, K.A. Andreassen, E.A. da Silva, C.E. Borba, C.A. Grande, Pressure swing adsorption for biogas upgrading with carbon molecular sieve, Ind. Eng. Chem. Res. 57 (2018) 8057–8067.
[31] B.J. Maring, P.A. Webley, A new simplified pressure/vacuum screening swing adsorption model for rapid adsorbent for CO2 capture applications, Int. J. Greenhouse Gas Control. 15 (2013) 16–31.
[32] M.G. Plaza, S. García, F. Rubiera, J.J. Pis, C. Pevida, Post-combustion CO2 capture with a commercial activated carbon: Comparison of different regeneration strategies, Chem. Eng. J. 163 (2010) 41–47.
[33] S. Brunauer, P.H. Emmett, E. Teller, Desorption of gases in multimolecular layers, J. Am. Chem. Soc. 60 (1938) 309–319.
[34] B.C. Lippens, J.H. de Boer, Studies on pore systems in catalysts: V. The t method, J. Catal. 4 (1965) 319–323.
[35] D.M. Ruthven, Principles of adsorption and adsorption processes, 1th ed, John Wiley & Sons, New York, 1984.
[36] E. Glueckauf, Formulae for diffusion into spheres and their application to chromatography, J. Chem. Soc. 51 (1955) 1540–1551.
[37] M. Capocelli, M. Luberti, S. Inno, F. D'Antonio, F. Di Natale, A. Lancia, Post-combustion CO2 capture by RVPSA in a large-scale steam reforming plant, J. CO_2 Util. 32 (2019) 53–65.
[38] N. Susarla, R. Haghpanah, I.A. Karimi, S. Farooq, A. Rajendran, L.S.C. Tan, J.S.T. Lim, Energy and cost estimates for capturing CO2 from a dry flue gas using pressure/vacuum swing adsorption, Chem. Eng. Res. Des. 102 (2015) 354–367.
[39] W.E. Schiesser, G.W.A. Griffiths, Compendium of partial differential equation models: method of lines analysis with Matlab, Cambridge University Press, New York, 2009.
[40] P. Sarker, U.K. Chakravarty, A generalization of the method of lines for the numerical solution of coupled, forced vibration of beams, Math. Comput. Simulat. 170 (2020) 115–142.
[41] A. Pal, K. Uddin, B.B. Saha, K. Thu, H.S. Kil, S.H. Yoon, J. Miyawaki, A benchmark for CO2 uptake onto newly synthesized biomass-derived activated carbons, Appl. Energy 264 (2020) 114720.
[42] G. Singh, K.S. Lakhi, S. Sil, S.V. Bhosale, I.Y. Kim a, K. Albahily, A. Vinu, Biomass derived porous carbon for CO2 capture, Carbon 148 (2019) 164–186.
[43] S. Shahkarami, R. Azargohar, A.K. Dalai, J. Soltan, Breakthrough CO2 adsorption in bio-based activated carbons, J Environ. Sci. 34 (2015) 68–76.
[44] R.S. Ribeiro, A.M.T. Silva, J.L. Figueiredo, J.L. Faria, H.T. Gomes, The influence of structure and surface chemistry of carbon materials on the decomposition of hydrogen peroxide, Carbon 62 (2013) 97–108.
[45] H.T. Gomes, S.M. Miranda, M.J. Sampaio, A.M.T. Silva, J.L. Faria, Activated carbons treated with sulphuric acid: Catalysts for catalytic wet peroxide oxidation, Catal. Today 151 (2010) 153–158.
[46] J.L. Figueiredo, M.F.R. Pereira, M.M.A. Freitas, J.J.M. Órfão, Modification of the surface chemistry of activated carbons, Carbon 37 (1999) 1379–1389.
[47] B.E. Poling, M. Prausnitz, J.P. O'Connell, The properties of gases and liquids, 5th ed, Mc-Graw Hill, New York, 2001.